Fluid Dynamics and Aero-Optical Environment Around Turrets.

Stanislav Gordeyev and Eric Jumper,
Department of Aerospace and Mechanical Engineering,
University of Notre Dame, Notre Dame, IN 46556

A summary of research efforts for last several years on fluid-dynamics and aero-optics of hemisphere-on-cylinder turrets with flat or conformal windows is presented. A topology of flow behind turrets and both steady and unsteady sources of optical distortions are discussed. Scaling laws for levels of optical aberrations are proposed and results of several experimental studies are compared and discussed. Effects of passive and active flow control in mitigation of aero-optical environment around turrets, as well as current computational studies of aero-optics of turrets are summarized and discussed.

I. Introduction

FROM an optical point of view, hemisphere-on-cylinder turrets are optimal platforms with large fields-of-regard to project or receive laser beams to or from a target. Land-based observatories for telescopes are perfect examples of such turrets. But when the turret is placed on an airborne platform moving through the air at subsonic, transonic or supersonic speeds, it becomes apparent that turrets create complex flow patterns around them, which ultimately can impose serious optical aberrations on laser beam.

Airborne optical turrets were extensively studied in 1970s and early 1980s. It was concluded that for airborne laser of the day at low subsonic speeds turrets produce only steady-lensing aberrations and unsteady optical aberrations were found to be a contributing factor only at transonic and supersonic speeds, when unsteady density fluctuations become significant. Good summaries of extensive experimental and modeling efforts prior to the mid-1980s in studying optical turrets at transonic and supersonic speeds can be found in [1,2].

One of the main reasons why turrets were considered optically-inactive at low speeds is that the far-field pattern depends on a relative phase distortion, $\phi = 2\pi OPD(x,y)/\lambda$, where $OPD(x,y)$ is the Optical-Path-Difference of a distorted wavefront and λ is the laser wavelength; the Large-Aperture-Approximation provides an approximation for on-axis Strehl ratio, SR,

$$SR = \exp(-\sigma_\phi^2) = \exp(-(2\pi OPD_{rms}/\lambda)^2), \quad (1)$$

where σ_ϕ is the spatial root-mean-square of the relative phase distortion. In the 1970s most of the calculations were made for CO_2-lasers with the wavelengths of interest around 10 μm. Since 1980s, advances in laser technology made near-IR lasers (with wavelengths ~ 1μm) good candidates to be used for airborne laser. So, while *absolute* optical distortions are relatively small around turrets at moderate subsonic speeds (OPD_{rms} ~ 0.1 μm), *relative* phase distortions imposed on a much-shorter-wavelength laser beams were increased ten-fold or so, thus making unsteady optical distortions, caused by a separated flow behind a turret large enough to significantly reduce the far-field intensity.

In addition, there has been steady progress in wavefront measurement instrumentation. Now wavefront sensors can accurately measure wavefronts at sampling rates of up to ~100 kHz with good (thousands of sub-apertures) spatial resolution. Also some sensors can measure other important aerodynamic properties like the convective speeds of the aberrating structures in the flow[3]. All these reasons have lead to a renewed interest in recent years in studying and mitigating optical aberrations caused by turrets.

This paper summarizes and analyses recent efforts to investigate the fluid dynamics (Section II) and optical environments (Section III) around side-wall-mounted hemisphere-on-cylinder turrets with either conformal or flat windows at moderate Mach numbers between 0.3 and 0.5, intentionally leaving other turret configuration, like nose-mounted turrets outside of the scope of the paper. The latest results in improving optical aberrations via active or

passive flow control (Section IV) and computational efforts to correctly predict aero-dynamical and aero-optical properties around turrets (Section V) are summarized and discussed.

II. Fluid Dynamics of Turrets

Before presenting any results, some basic definitions of the turret parameters and angles should be introduced, see Figure 1. The turret is defined by its hemispherical diameter, D, and the cylindrical base height, H. The diameter of the aperture window is denoted as Ap. The direction of the outgoing laser beam emerging from the window relative to the incoming freestream flow is characterized by the azimuthal and the elevation angles, β and γ, respectively. It is also useful to introduce the window angle, α, defined as an angle between the outward beam-direction vector, normal to the window center and the freestream-direction vector, pointing upstream, see Figure 1. The relation between these angles is the following,

$$\cos(\alpha) = \cos(\beta)\cos(\gamma) \tag{2}$$

It is easy to see that, for instance, when the azimuthal angle is zero, the window angle coincides with the elevation angle, $\alpha = \gamma$ and if $\beta = \pi$, then $\alpha = \pi - \gamma$, thus the window angle goes from 0 to π when the beam-direction vector lies on the center-plane, defined as $\beta = 0$ or π. The window angle will be used in the paper to compare optical results between different turrets for different azimuthal and elevation.

The non-optimal aerodynamic shape creates a complex flow pattern around the turret, see Figure 2. It consists of a necklace vortex formed in front of the turret, with its "legs" extended downstream of the turret. The flow is attached at the front part of the turret, while the adverse pressure gradient at the back part of the turret forces the flow to separate. The separation region interacts with the necklace vortex and creates a complex three-dimensional region behind the turret. The surface flow topology around the conformal-window turret and the hemisphere at different Mach numbers are shown in Figure 3. At low Mach numbers, see Figure 3, left column, two counter-rotating vortices separating from the back part of the turret are clearly visible. At higher Mach numbers, the symmetry between these two vortices is broken and an even-more complex flow pattern at the back of the turret emerges, with either one large or several smaller vortices separating from the back of the turret, visible in Figure 3, right column.

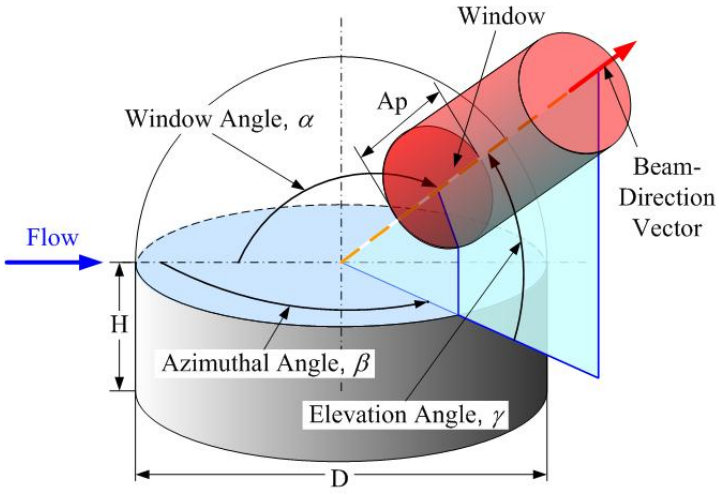

Figure 1. Definitions of geometric parameters and angles for a hemisphere-on-cylinder turret.

When the hemispherical part of the turret is well above the necklace vortex, the flow around it is similar to the flow around spheres. The flow around spheres at high Reynolds numbers was extensively studied[4]. It was found that when Re is less than 200,000, the boundary layer is laminar before separation and the separation occurs around the window angle of 80-85 degrees. When the Reynolds number is above 300,000, the separation point over a sphere moves to ~120 degrees due to a laminar-to-turbulent boundary-layer transition upstream of the separation point.

Surface static pressure measurements for different conformal-window turrets along the centerline are presented in Figure 4, left. Cp-data for a small turret[5] with Re_D = 190,000 revealed that laminar-boundary-layer separation occurs around 100 degrees, which is further downstream of the separation point at 82 degrees over the sphere[4]. Results for pressure distributions at $Re > 2\text{x}10^6$ for the different turret sizes, D = 12", H/D = 0.375, Re_D = 2.3M [6] and D = 24", H/D = 0.31, Re_D = 4.5x x10^6 [7] also shown in Figure 4, left. The Cp-distributions are nearly identical and independent of the Reynolds number. The flow stagnates at $\alpha = 0$ degrees, accelerates on the front portion of the turret, starts decelerating at the back portion and separates between 115 and 120 degrees, consistent with the separation location over a sphere. In the separated region the pressure is nearly constant at Cp = -0.3, regardless of the Reynolds number. This value is quite similar to the static pressure inside the separation region behind a sphere. A schematic of the flow topology around the hemisphere-on-cylinder turret is given in Figure 4, upper right.

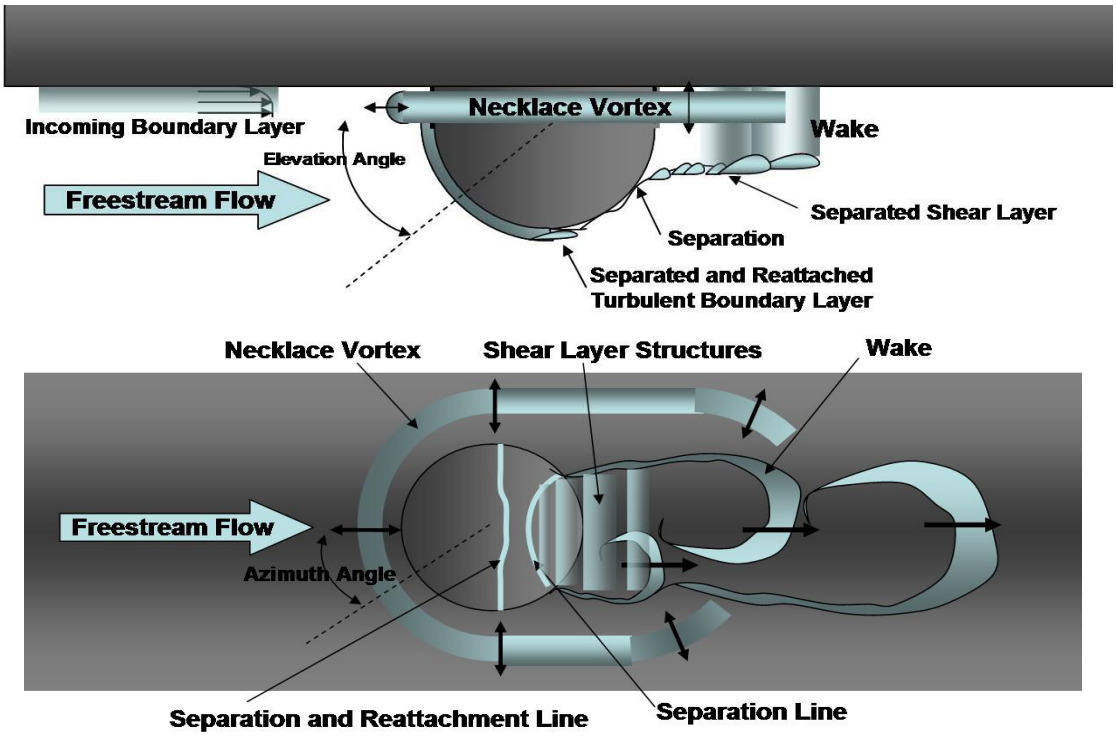

Figure 2. Schematic of the flow around the turret.

When only the hemisphere is placed on the surface[8], that is $H = 0$, the presence of the necklace vortex changes the Cp-distribution around the hemisphere, see Figure 4, left. The necklace vortex pushes the stagnation point in front of the hemisphere to approximately $\alpha = 15$ degrees. The Cp-value on top of the hemisphere ($\alpha = 90$ degrees) is slightly lower than on top of the turret. The flow also separates around 120 degrees, but the Cp-values are not constant inside the separated region, although Cp eventually reaches the same value as for the turret case of Cp = -0.3, at $\alpha > 140$ degrees. The schematic of the flow is given in Figure 4, lower right.

In Figure 4, right, the Cp-distribution for the potential flow around the sphere,

$$Cp(\alpha) = 1 - 9/4 \sin^2(\alpha), \quad (3)$$

is also plotted. For the hemisphere-on-cylinder configuration, the necklace vortex is well below the hemispherical part of the turret and the potential Cp-solution Eq. (3) describes quite well the pressure distribution on the front part of the turret. For the hemisphere, as mentioned before, the necklace vortex is present at the bottom of the hemisphere, thus slightly changing the Cp-distribution away from the potential solution. Similar results were also observed by other researchers[9].

So, the static pressure results on the center-plane are very similar to the results over spheres for high Re-numbers. But, due the presence of the surface and the necklace vortex at the bottom of the turret, the separated region behind the turret cannot be simply modeled as the separated region behind a sphere. The surface flow topology on turrets, presented in Figure 3, clearly indicates the presence of large-scale vortices separating from the back of the turret. The separation line was shown to depend on the elevation angle[7]. Finally, we know that the critical Reynolds number for laminar-to-turbulent boundary layer transition on a sphere is reported to be ~ 300,000 [4], and we have seen data, as reported earlier, that shows that transition on a turret is at essentially the same Reynolds number, while other turrets studies have shown a transition at Reynolds numbers as high as 500,000; this is mentioned here as precautionary note, primarily in attempting to extrapolate data from just over 300,000 to higher Reynolds number applications.

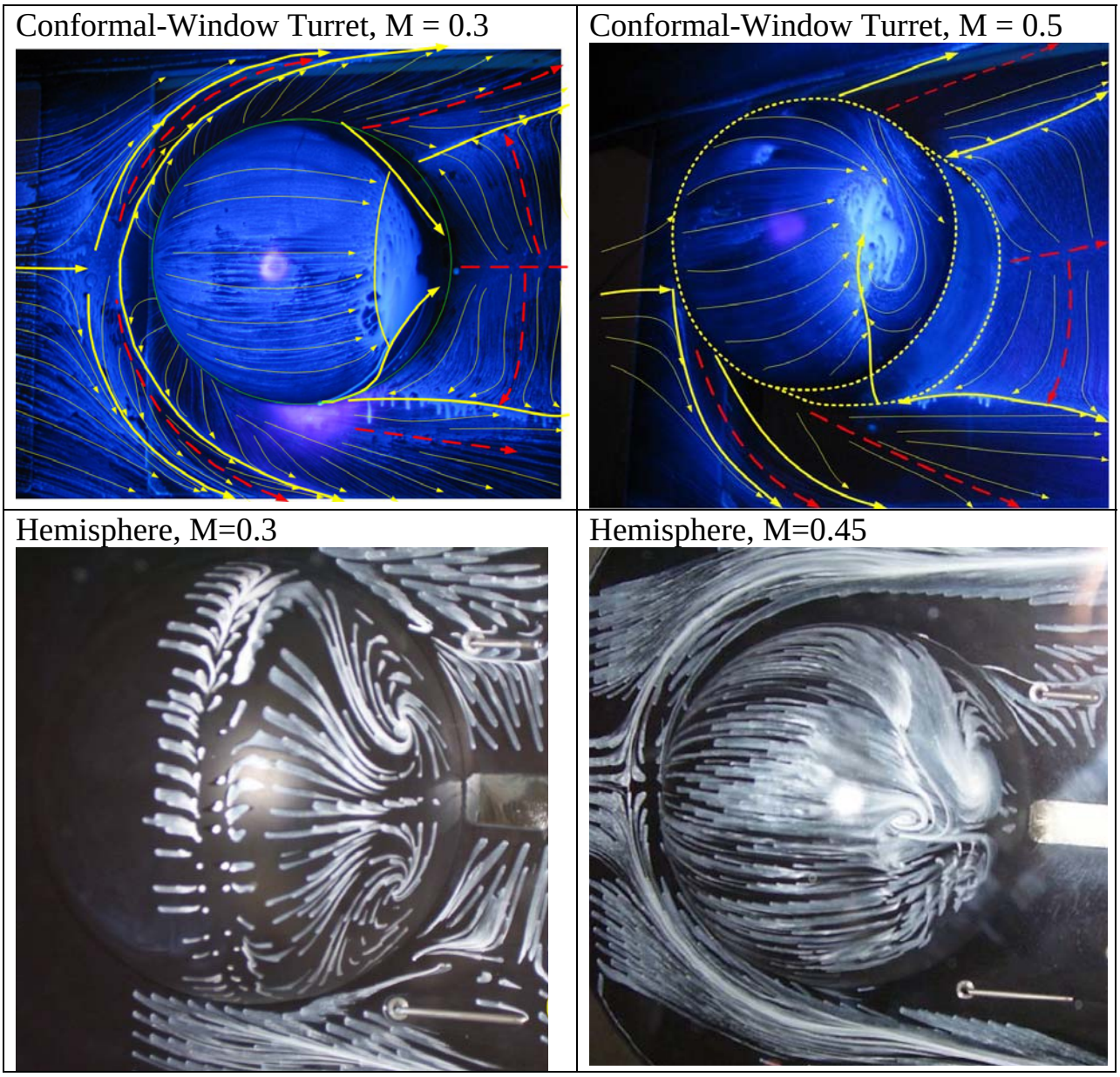

Figure 3. Surface flow topology on different turrets: Conformal window turret at M = 0.3, Re_D = 2.3x10^6 (upper left) and M = 0.5. Re_D = 3.9x10^6 (upper right) (from [6]) and hemisphere at M = 0.3, Re_D = 2x10^6 (lower left) and M=0.45, Re_D = 2.9x10^6 (lower right) (from [8]).

In the case of flat-window turrets the flow becomes viewing-angle-dependent due to the slope discontinuity around the window, thus adding an extra layer of complexity to an already complicated flow topology behind turrets. Unfortunately, only a few limited open literature experimental studies of the flow topology (and aero-optical properties) around the flat-window turrets are available, mostly in the 1970s and early 1980s.[1]

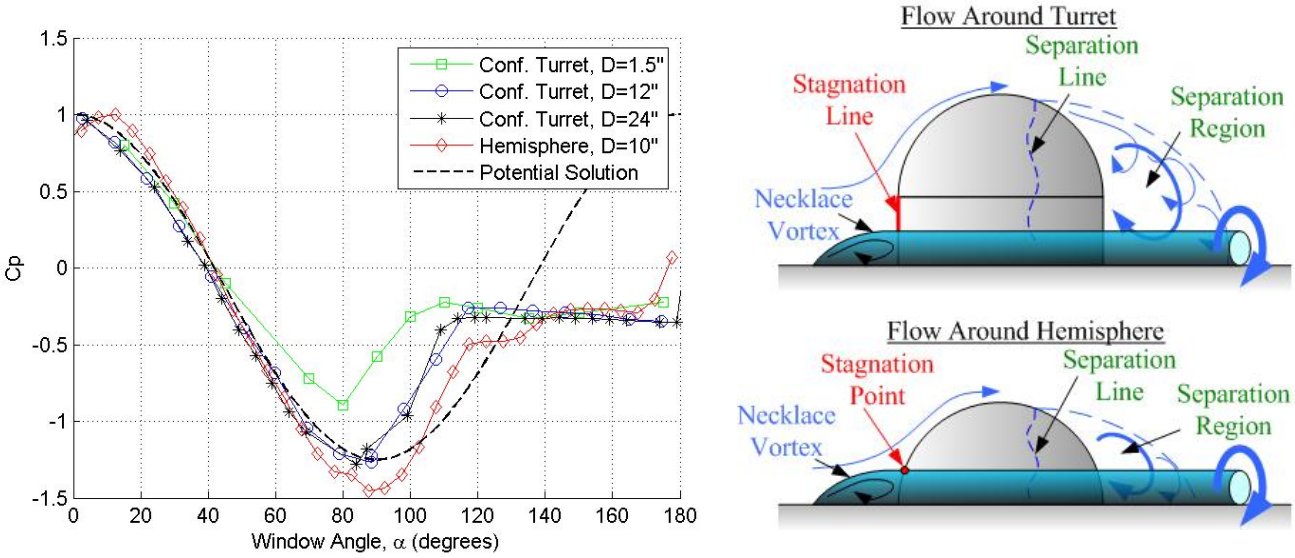

Figure 4. Left: Pressure coefficients along the turret's center-plane, compensated for blockage, for conformal-window turret, D = 1.5", H/D = 0.3, Re_D = 190,000, (from [5]), conformal-window turret, D = 12", H/D = 0.375, $Re_D = 2.3\times10^6$ (from [6]), conformal-window turret, D = 24", H/D = 0.31, $Re_D = 4.5\times10^6$ (from [7]) and hemisphere, D = 10" $Re_D = 2.6\times10^6$ (from [8]). The potential solution for the flow around a sphere (3) is given as a dashed line. Right: the schematic of the flow topology around the hemisphere-on-cylinder turret and the hemisphere.

III. Optical results

Forward-looking angles.

As discussed in the previous section, flow around the forward half of the conformal-window turret is attached and it can be fairly accurately described by a potential inviscid flow solution around a sphere,

$$u_r(r,\alpha) = U_\infty \sin(\alpha)\left[1-\left(\frac{R}{r}\right)^3\right], \quad u_\alpha(r,\alpha) = -U_\infty \cos(\alpha)\left[1+\frac{1}{2}\left(\frac{R}{r}\right)^3\right], \tag{4}$$

where u_r and u_α are the radial and the window-angle velocity components, r is the distance from a point in the flow from the sphere center, U_∞ is the freestream velocity and $R = D/2$ is the sphere radius. Knowing the velocity distribution in space, the density variations can be estimated assuming weakly-compressible flow; the velocity field creates pressure variations through Bernoulli equation, $p'+1/2\rho_0(u_r^2+u_\gamma^2) = p_0 = const$ and the density and pressure are related via an anisotropic equation, $\gamma\rho'/\rho_0 = p'/p_0 = p'/(\rho_0 c^2)$, where c is a speed of sound. Finally, the density field can be integrated along the lines parallel to the beam-propagation direction starting at the aperture to get so-called *steady-lensing* optical aberrations due to a nearly-steady density field around the turret,

$$OPD_{steady} \sim K_{GD}\int_a^\infty \rho'(\vec{x})dl \sim -K_{GD}\left(\frac{1}{2c^2}\rho_0\right)\int_a^\infty u^2(\vec{x})dl \sim -K_{GD}\left(\frac{U_\infty^2}{2c^2}\rho_0 R\right)\int_a^\infty f(r/R,\alpha)d(l/R) \tag{5}$$

$$OPD_{steady} = (\rho_0/\rho_{SL})M^2 D\ f(Ap/D,\alpha)$$

where $f(\mathrm{Ap}/D,\alpha)$ is a function of the relative aperture size and the window angle. It follows from Eq. (5) that the steady-lensing optical aberrations scale as $OPD_{steady} \sim \rho_0 M^2 D$. Examples of "normalized" wavefronts, $f(\mathrm{Ap}/D,\alpha)$, for several forward-looking window angles in the center-plane for Ap/D = 0.33 are shown in Figure 5.

For simple turret geometries, like the hemisphere-on-surface, the potential approach was extended[10] to transonic and supersonic flows to calculate the steady-lensing wavefronts.

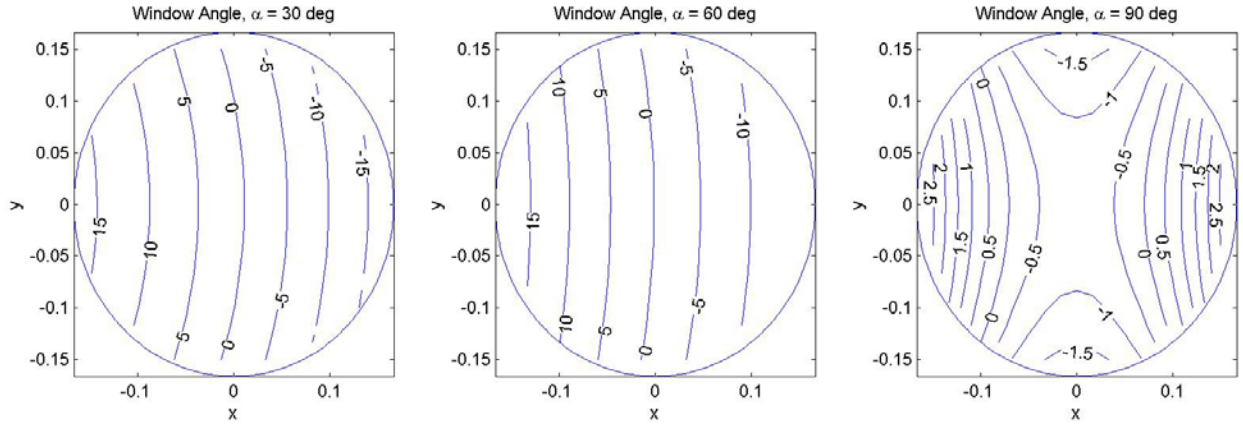

Figure 5. Steady lensing normalized wavefronts, defined in (5) for several forward-looking window angles around the sphere.

Although the flow is attached to the turret's surface for forward-looking angles, optical aberrations, in addition to the steady-lensing part, also have unsteady components. The laser beam is transmitted *directly* through the attached boundary layer, which itself has been shown to be a source of unsteady optical aberrations at high subsonic speeds[11- 13]. The second source of unsteadiness is the necklace vortex at the bottom of the turret and the unsteady separated region behind the turret, which *indirectly* affect the pressure and density field *everywhere* around the turret via Biot-Savart induction mechanism and unsteady necklace movement which has been correlated to the unsteadiness in the wake. Evidence of these indirect effects on the optical aberrations was experimentally observed around the conformal-window turret[6].

The flow around the flat-window turret is more complex due to the surface-slope discontinuity around the aperture window, so the potential solution approach Eq. (5) will not work to estimate steady-lensing effects for forward-looking angles. Also, the slope discontinuity can create local separation/re-attachment regions over the flat window, which is an additional source for unsteady optical aberrations. This effect is yet to be experimentally studied to any depth.

Back-looking angles.

When the beam is directed backward, it is transmitted through the separated shear layer behind the turret. For large turrets, the separation occurs around 115-120 degrees, so for any window angles above this value, large-scale vortical structures inside the separated shear layer become the main source of the unsteady optical distortions and severely limit the performance of turret-based lasers at back-looking angles.

To properly analyze experimental results, it is important to understand the scaling of these aberrations. Let's recall that Optical Path Length OPL is an integral of the index-of-refraction along a laser ray,

$$OPL(x) = \int n(x)ds = \int n_0(1 + K_{GD}(\rho - \rho_0)/n_0)ds,$$

where for the air $K_{GD} \cong 0.000227$ m^3/kg is the Gladstone-Dale constant and ρ_0 is a freestream density. From here it follows that the Optical path Difference, *OPD*, is proportional to the integral of the density variations through the turbulent field,

$$OPD(x) \sim \int (\rho - \rho_0)ds$$

For isentropic flows, $\Delta p/p_0 \sim \gamma \Delta\rho/\rho_0$, and, noting that the pressure drop inside a vertical structure of size θ with a characteristic velocity u is $\Delta p \sim \rho_0 u^2 \sim p_0/T_0 u^2 \sim p_0 (u/c)^2 \sim p_0 M^2$, we get the following expression for the variations in *OPD*,

$$OPD_{rms} \sim OPD \sim \theta \rho_0 M^2,$$

where M is the convective Mach number and c is a freestream speed of sound. Thus, optical aberrations due to vortical structures depend linearly on the freestream density and the structure size and the square of the convective Mach number. This 'ρM^2'-dependence of the level of optical distortions was proven to be correct for most the turbulent flows for subsonic speeds[3, 6-8, 13].

In general, optical aberrations depend on the incoming-boundary layer thickness, δ, a typical vortical structure size/scale θ, the turret diameter, D, the cylindrical base height, H, the beam aperture, A_p, the freestream density, ρ_0, the freestream Mach number, M, the Reynolds number, Re, the window type (flat or conformal) and the viewing angles, α and β.

$$OPD_{rms} = f(\delta, \theta, D, H, A_p, \rho_0, M, \mathrm{Re}, \alpha, \delta) \tag{6}$$

Using Eq. (6) and applying dimensional analysis, we can get the following relationship for the OPD_{rms},

$$\frac{OPD_{rms}}{D} = \frac{\theta}{D}\frac{\rho_0}{\rho_{SL}} M^2 g\left(\frac{A_p}{D}, \frac{\delta}{D}, \frac{H}{D}, \alpha, \beta, \mathrm{Re}\right), \tag{7}$$

For a sufficiently small incoming boundary layer, $\delta/D << 1$, most of the boundary layer on the turret-mounting surface upstream of the turret gets wrapped into the necklace vortex and does not *directly* effect optical distortions over the turret. A new boundary layer on the hemispherical portion of the turret starts re-growing from the stagnation point in front of the turret. Therefore, the boundary-layer thickness before it separates from the turret will be proportional to the turret diameter only; therefore the large-scale structure inside the separated shear layer, θ, will also be proportional to the turret diameter, $\theta/D \cong$ const.

When the Reynolds number is smaller then the critical number, $Re < Re_C$, the boundary layer on the turret is laminar and the separation point is located around α = 100 degrees. When $Re > Re_C$, the boundary layer becomes turbulent before it separates and the separation point moves to approximately α = 115-120 degrees, see Figure 4. The main mechanism for creating the large-scale structures inside the separated shear layer, which have been shown to be the main source for the optical distortions[14,15], is the inviscid inflectional mechanism, which is mostly independent of Re; the Reynolds number affects only the small structures in the shear layer which typically do not add any significant optical distortions. Therefore, as long as the Reynolds number is greater than the critical value, the optical distortions usually do not depend on Re. Therefore, the proposed scaling Eq. (7) can be re-written as,

$$\frac{OPD_{rms}}{(\rho_0/\rho_{SL})M^2 D} = A\left(\frac{H}{D}, \frac{A_p}{D}, geometry\right) B(\alpha, \beta) \tag{8}$$

where A is a function of the turret shape, H/D, and the geometrical turret shape (like the flat window versus the conformal window, for example), as well as the relative aperture size, A_p/D. If the relative aperture size is the same between different experiments, A becomes a function of the turret shape only. B is a function of the window and viewing angle only.

For looking-back angles, α > 90 degrees, the laser beam travels a longer distance through the separated region of the flow behind the turret, and it is reasonable to assume that the optical aberration will be proportional to this distance. As a first approximation, the azimuthal-angle-dependence can be neglected; i.e., B = 1 in Eq. (4); however, it has been proposed that a better value for B is $B = 1/\sin(\alpha)$, similar to the observed oblique-viewing-angle dependence, observed for the turbulent boundary layers[13] and separated shear layers[16].

To check the proposed scaling of Eq. (8), optical results from several tests for different turret with different shapes (conformal window[6,7], flat window[15]) and different H/D over a range of back-looking angles are plotted in Figure 6. The relative window aperture was the same for all turrets, A_p/D = 0.33. All optical results were corrected for the tunnel blockage. "A/sin(α)" – fits are also plotted in Figure 6 for different experiments. The "oblique-angle" approximation, 1/sin(α), at least empirically, provides a good fit to all the available data. Clearly, the function A depends on the turret geometry: A = 0.95 μm/m for the conformal-window turrets, A = 1.75 μm/m for the flat-window turrets and A = 2.1 μm/m for the hemispheres-on-surfaces.

Several important observations can be drawn from Figure 6. One observation is that somewhat contrary to a conventional thinking, the less-protruding hemisphere-on-surface provides the worst optical environment, while the more-protruding hemisphere-on-cylinder turret (with H/D = 0.33) is more that twice better aero-optically. One possible explanation is that for the hemisphere-on-surface, the necklace vortex is closer to the aperture window and has a greater indirect effect on the laser beam. Another observation is that the flat-window turret is always aero-optically worse that the conformal-window turret, although there is no experimental data available to see whether optical aberrations for the flat-window turret and the conformal-window turret would converge for large window angles above 150 degrees, when the flat-window aperture is completely inside the separated flow behind the turret.

Results for a small cylindrical turret with a flat window[17] are also presented in Figure 6 and they follow the "1/sin(α)" –approximation with A = 1.4 μm/m. As discussed in detail in [15], the aero-optical environment around a

simplified 2-D flat-window turret is quite similar and relevant to the environment around a 3-D flat-window hemisphere-on-cylinder turret, since the two share the same unsteady source of the optical aberrations - a separated flow over the flat-window; therefore, the flow around the cylindrical turret with the flat window becomes an important benchmark experiment to validate different aero-optical computational codes.

The final note about the optical environment around different turrets for back-looking angles is that Figure 6 presents almost all data available in the open literature; yet, there are only 7 points for the conformal-window turrets along the center-plane only, 4 points for the flat-window turret for one elevation angle and 4 points for the hemisphere, also along the center-plane only. No doubt, more experimental data are required to completely quantify and understand the optical environment around turrets for different elevation and azimuth angles, even at low subsonic speeds.

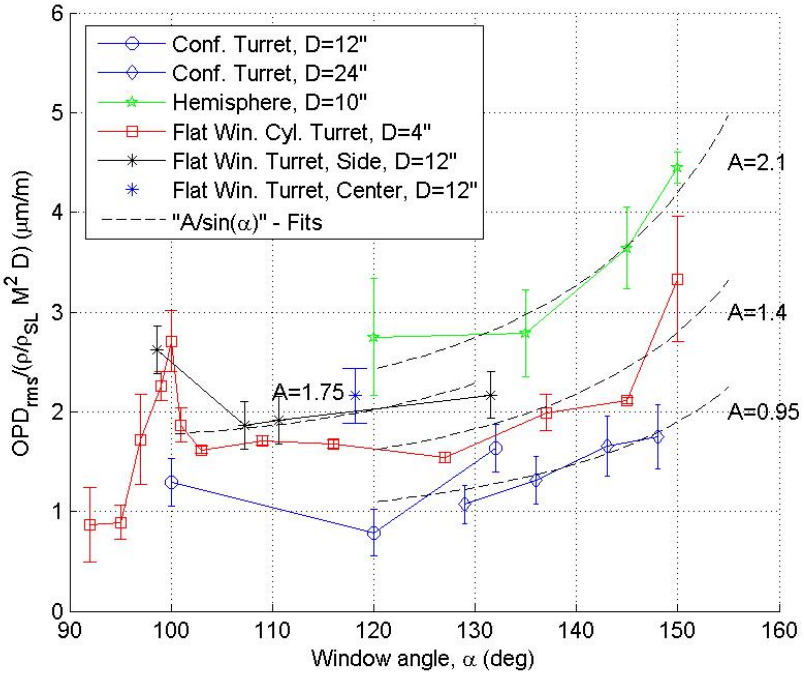

Figure 6. Levels of optical distortions, OPD_{rms} , normalized by (ρ/ρ_{SL}) M^2 D for different turrets as a function of the window angle, α, defined in (1): conformal-window turret, D = 12", H/D = 0.375, center-plane, (from [6]), conformal-window turret, D = 24", H/D = 0.31, center-plane (from [7]), hemisphere, D = 10", H/D = 0, center-plane (from [8]), flat-window cylindrical turret, D = 4" (from [17]), flat-window turret, D = 12", H/D = 0.375, γ = 30 degrees (from [15]). Aperture size is 1/3 of the turret diameter for all cases. "A/sin(α)"-fits are shown as dashed lines with different constants A, defined in (8).

IV. Effect of Flow Control on Optical Distortions

As it was discussed in the previous Section, optical aberrations are significant for large turrets and large back-looking angles. As an example, consider a laser beam directed at a window angle of 150 degrees from the least-aberrating conformal-window turret with D = 1m flying at the sea-level at a relatively low speed of M = 0.3. From Figure 6 experimental data for conformal-window turrets gives A = 0.95 μm/m. Using Eq. (8), the level of optical aberrations would be OPD_{rms} = 0.17 μm and the far-field Strehl ratio Eq. (1) for λ = 1 μm is found to be SR = 0.31. In other words, 70% of the diffraction-limited laser energy on a target will be lost.

The main source of large optical distortions is the separated turbulent region downstream the turret, and one way to mitigate aero-optical problems and increase the far-field Strehl ratio is to reduce the separation region or modify it to make it less optically active. This can be accomplished with either passive or active flow control.

A variety of different passive-flow control devices have been tested to minimize the separation region; they included fairings behind the turret, which are known to reduce aerodynamic drag, but were largely ineffective in significantly improving the aero-optical problem[18]. Fairings were also used to provide steady suction behind the turret to reduce wake unsteadiness[19,20]; while some flow improvements were achieved, no optical measurements were taken. Several experiments[1,15] tested different fences and vortex generators around the aperture in an attempt to

delay the natural separation off the turret; most of these studies showed that at large back-looking angles only marginal reductions in optical distortions were achieved.

Having said that, it is worth mentioning that some passive control devices are promising candidates for improving aero-optical environments around flat-window turrets at moderate back-looking angles, where the presence of the slope-discontinuity around the window causes premature flow separation and subsequent increases in OPD_{rms}[15]. When a single row of small pins was placed upstream of the window, they energized the boundary layer and forced the flow to re-attach, reducing the separation bubble over the flat window and concomitantly lowering levels of optical distortions, see Figure 7.

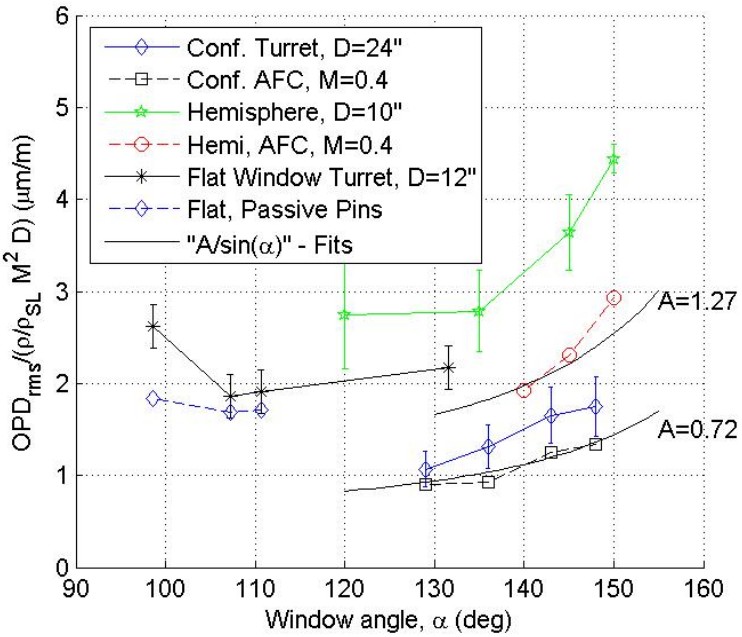

Figure 7. Effect of different passive or active flow control (AFC) devices on the level of optical distortions, OPD_{rms} , normalized by (ρ/ρ_{SL}) M^2 D for different turrets as a function of the window angle, defined in (1): conformal-window turret, D = 24", center-plane, baseline and with AFC (synthetic jets upstream of the window) (from [7]), hemisphere, D = 10", center-plane, baseline and with AFC (synthetic jets upstream of the window) (from [8]), flat-window turret, D = 12", baseline and passive pins upstream of the window, elevation angle is 30 degrees (from [15]). Aperture size is 1/3 of the turret diameter for all cases. "A/sin(α)"-fits are shown as dashed lines with different constants A, defined in (8).

With the development of compact and more-powerful active flow control devices over the last decade, active flow control has been used to modify the separation bubble by delaying the separation point and/or modifying the separated shear layer. Rows of synthetic jets pulsating at high frequencies[21] were used upstream of the window on a conformal-window hemisphere-on-surface[8] and shown to significantly improve optical distortions at relatively-large back-looking angles. Figure 7 presents normalized levels of optical aberrations for the baseline (no actuation) and controlled cases (with actuation) in the hemisphere-on-surface tests[8]. The empirical curve-fit "A/sin(α)" is also plotted in Figure 7. The optical environment behind the hemisphere was reduced by as much as 40%, from A = 2.1 μm/m for the baseline (Figure 6), down to A = 1.27 μm/m (Figure 7) for the controlled cases. Similar reductions were found for conformal-window hemisphere-on-cylinder turrets[7], from A = 0.95 μm/m for the baseline, shown in Figure 6, to A = 0.72 μm/m (25% reduction). So, if the same example in the beginning of this Section is used, active flow control with synthetic jets would reduce OPD_{rms} to 0.13 μm and increase the Strehl ratio up to 0.51. There is some data that shown that a further reduction in OPD_{rms} can be achieved by combining passive and active flow control strategies.

As a final remark on the active flow control approaches, several *closed-loop* active-flow-control algorithms were recently developed[22, 23]. They use unsteady pressure sensors placed on the surface of the flat-window turret as a feedback into a POD-based model to drive pulsating synthetic jets upstream of the window. The closed-loop control

algorithm was designed to reduce surface pressure fluctuations. No direct optical data are available yet, but the levels of surface unsteady pressure, which are believed to be linked to optical aberrations[8], were reduced by 18% and it was observed that the actuation drives the flow toward homogeneity.

V. Computational Efforts to Predict the Fluid Dynamics and Aero-Optical Aberrations of Turrets.

Aero-optical problems are computationally difficult, because they are required to properly resolve small-scale unsteady density fluctuations in the flow. The flow around a turret is particularly computationally challenging, since it has a large range of vortical structures that must be properly resolved, which range from the order of the turret diameter (the necklace vortex and the separation region) down to small vortical structures in the separated shear layer. The density field must be resolved both temporally and spatially, so steady RANS models cannot be used. Also, typical Reynolds numbers for turrets are in the millions and Direct Numerical Simulations (DNS) would require prohibitive amount of computational resources to compute the flow.

In one of the first attempts[24] to calculate the unsteady compressible flow around a turret, a Cebeci-Smith type eddy viscosity model was used to solve unsteady N-S equations. In a different study[25], the unsteady density field around a partially protruding hemisphere with a flat window was obtained from the CFD analysis and they were used to perform aero-optical analysis of laser beams propagating from the turret.

Recently, several LES-based codes were constructed and validated against experimental results. A CFD-based validation study using a k-ε turbulence model with an unsteady partially-averaged Navier-Stokes (PANS) solver was conducted[5]; this study was shown to correctly predict aerodynamic and aero-optical environment around small and large conformal-window turrets, see Figure 8. An implicit Large-Eddy-Simulation (ILES), 6th-order solver was developed[26] which was compared against experiments[6]. Many features of the flow were properly predicted, although some differences were noted in the separation region. A modification of this code, a hybrid RANS/ILES solver[27] was used to predict the flow around a conformal-window turret at M = 0.4 and $Re_D = 2.4x10^6$. This code was also used to test the effectiveness of different suctions on the turret, see Figure 9. An unsteady Reynolds-Averaged Navier-Stokes (RANS) model and a blended Large Eddy Simulation (LES) with two-equation turbulence model[28] were evaluated to predict aerodynamics and aero-optics of the turrets. Aerodynamic predictions of time-averaged turret surface pressures and several downstream velocity profiles showed good agreement with experiments. Aero-optical quantities were also compared fairly well with experiment through a range of elevation angles, see Figure 10.

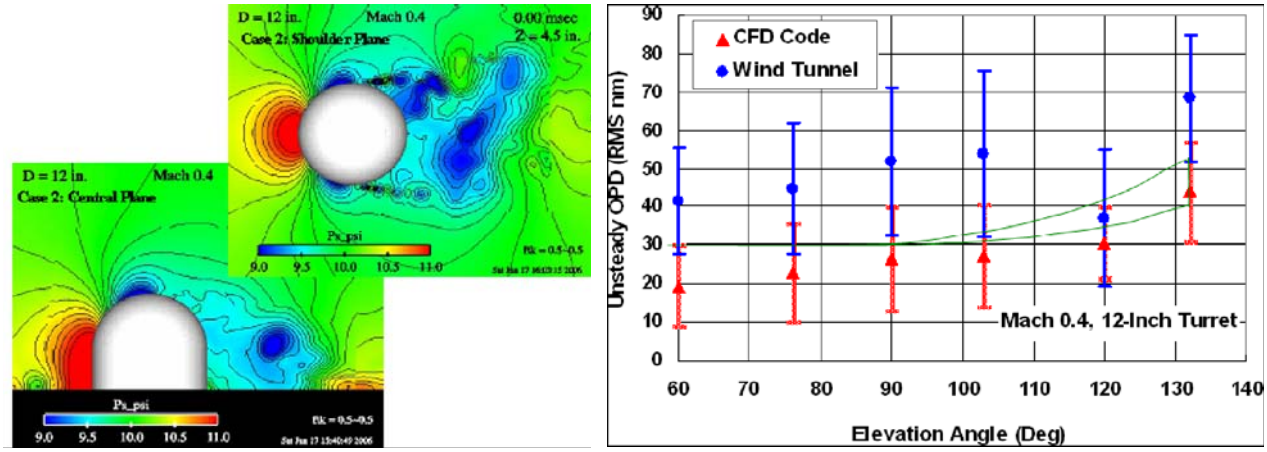

Figure 8. Left: Snapshots of flow-field around the turret (from [5]). Right: Comparison of levels of optical aberrations between experiments [6] and CFD [5].

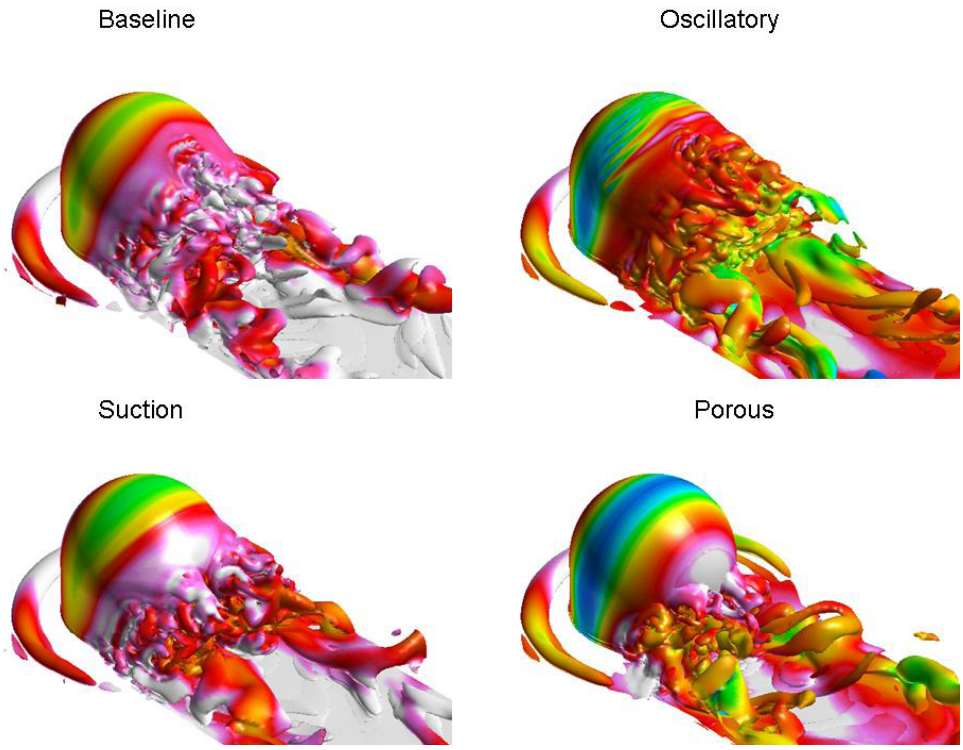

Figure 9. Numerical simulations of the flow around the turret and effects of porous suction (from [27])

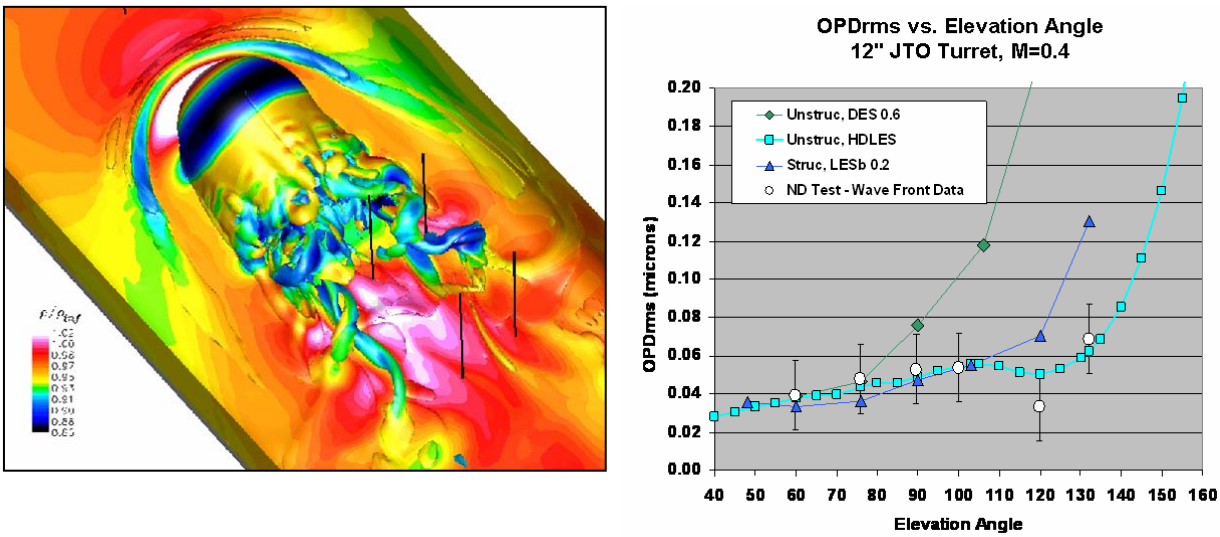

Figure 10. Left: Flow around the turret with a conformal window. Right: Comparison of OPDrms with experiments (from [28]).

All the cited CFD studies dealt with flow around conformal-window, hemisphere-on-cylinder turrets, which do not depend on the viewing angle; thus, the same numerical solution can be used to calculate the optical distortions at different viewing angles, since it only requires post-integrating along the beam. The flat-window turret, on the other hand, would require a separate numerical simulation for each viewing angle, thus making the computational predictions very expensive. To the authors' knowledge, there are no available numerical simulations that predict aero-optics of the flat-window turrets at realistic Reynolds numbers.

To conclude this brief discussion of aero-optic-related CFD efforts, it is important to note again that due to geometrical simplicity and relevance to aero-optical problems[15], the experimental results for the flow and aero-optical aberrations around a 2-dimensional, cylindrical turret[17] provide excellent benchmark experimental data to validate CFD studies[29-31].

VI. Final Remarks.

This paper is really a first attempt at trying to bring together what is now known about airborne optical turrets; there is bound to be information we have overlooked. Even so, this paper has demonstrated the fact that after decades of studying this problem, there is still a paucity of experimental and computational data on this important airborne-laser geometry. An encouraging sign is that the level of research efforts picked up in the last years: a simple search for word "turret" in AIAA database revealed only 6 references prior to 1983, no papers between 1984 and 1999, and a burst of publications in the last few years, with 17 papers in the last three years alone. No doubt, many exciting discoveries on this important area of aero-optical research, both fundamental and applied, will be made.

References

[1]Gilbert KG, Otten LJ, editors. *Aero-Optical Phenomena, Progress in astronautics and aeronautics series*, Vol. 80. New York: American Institute of Aeronautics and Astronautics, 1982.

[2]Sutton, G.W., "Aero-Optical Foundations and Applications, *AIAA Journal*, Vol. **23**, pp. 1525-1537, 1985.

[3]S. Gordeyev, T. Hayden and E. Jumper, "Aero-Optical and Flow Measurements Over a Flat-Windowed Turret", AIAA Journal, vol. 45, No. 2, pp. 347-357, 2007.

[4]E. Achenbach "Experiments on The Flow Past Spheres at Very High Reynolds Numbers," *J. Fluid Mech.*, Vol. **5**4(3), 1972, pp. 565-575.

[5]D. Nahrstedt, Y-C. Hsia, E. Jumper, S. Gordeyev, J. Ceniceros, L Weaver, L DeSandre and T. McLaughlin," Wind Tunnel Validation of Computational Fluid Dynamics-Based Aero-Optics Model," *Proc. IMechE, Part G: J. Aerospace Engineering*, 2009, **223**(G4), pp. 393-406.

[6]S. Gordeyev, M. Post, T. MacLaughlin, J. Ceniceros and E. Jumper, "Aero-Optical Environment Around a Conformal-Window Turret", *AIAA Journal*, vol. **45**, No. 7, pp. 1514-1524, 2007.

[7]B. Vukasinovic, A. Glezer, S. Gordeyev, E. Jumper and V. Kibens "Fluidic Control of a Turret Wake, Part I: Aerodynamic Effects", 47th Aerospace Science Meeting and Exhibit, Orlando, Florida, 5-8 Jan, 2009, AIAA Paper 2009-0816.

[8]B. Vucasinovic, A. Glezer, S. Gordeyev, E. Jumper and V. Kibens, "Active Control and Optical Diagnostics of the Flow over a Hemispherical Turret", 46th Aerospace Science Meeting and Exhibit, 2008, AIAA Paper 2008-0598.

[9]R. Sluder, L. Gris and J. Katz, "Optical Turret Aerodynamics - a Preliminary Study", 46th AIAA Aerospace Sciences Meeting and Exhibit, 2008 AIAA Paper 2008-429.

[10]Fuhs, A.E and Fuhs, S.E. , "Optical phase Distortion due to Compressible Flow over Laser Turrets," in *Aero-Optical Phenomena*, Eds. K.G. Gilbert and L.J. Otten, Vol. 80, *Progress in Astronautics and Aeronautics*, AIAA, New York, 1982, pp. 101-138.

[11]S. Gordeyev, E. Jumper, T. Ng and A. Cain, "Aero-Optical Characteristics of Compressible, Subsonic Turbulent Boundary Layer", 34th AIAA Plasmadynamics and Lasers Conference, Orlando, Florida, 23-26 June, 2003, AIAA Paper 2003-3606.

[12]D. Wittich, S. Gordeyev and E. Jumper, "Revised Scaling of Optical Distortions Caused by Compressible, Subsonic Turbulent Boundary Layers", 38th AIAA Plasmadynamics and Lasers Conference, Miami, Florida, 25-28 June, 2007, AIAA Paper 2007-4009.

[13]J. Cress, S. Gordeyev, M. Post and E. Jumper "Aero-Optical Measurements in a Turbulent, Subsonic Boundary Layer at Different Elevation Angles", 39th Plasmadynamics and Lasers Conference, Seattle, Washington, 23 - 26 June, 2008, AIAA Paper 2008-4214.

[14]Fitzgerald, E. J. and Jumper E. J., "The optical distortion mechanism in a nearly incompressible free shear layer," *J. Fluid Mech.*, Vol. **512**, 2004, pp. 153-189.

[15]J. Cress, S. Gordeyev, E. Jumper, T. Ng and A. Cain, "Similarities and Differences in Aero- Optical Structure over Cylindrical and Hemispherical Turrets with a Flat Window", 45th Aerospace Science Meeting and Exhibit, Reno, Nevada, 8-11 Jan, 2007, AIAA Paper 2007-0326.

[16]D. Duffin,"Feed-Forward Adaptive-Optic Correction of a Weakly-Compressible High-Subsonic Shear Layer," Ph.D. Thesis, University of Notre Dame, Notre Dame, IN, 2009.
[17]S. Gordeyev, E. Jumper, T. Ng and A. Cain, "The Optical Environment of a Cylindrical Turret with a Flat Window and the Impact of Passive Control Devices", 36th AIAA Plasmadynamics and Laser Conference, Toronto, Canada, 6-9 June, 2005, AIAA Paper 2005-4657.
[18]Otten, L.J and Gilbert, K.G., "Inviscid FlowField Effects: Experimental Results," in *Aero-Optical Phenomena*, Eds. K.G. Gilbert and L.J. Otten, Vol. 80, *Progress in Astronautics and Aeronautics*, AIAA, New York, 1982, pp. 233-241.
[19]J. R. Schonberger, A. E. Fuhs and A. M. Mandigo," Flow Control for an Airborne Laser Turret," *Journal of Aircraft*, 1982, Vol.**19**, No.7, pp. 531-537.
[20]Purohit, S. C. and Shang, J. S., "Effect of suction on the wake structure of a three-dimensional turret," American Institute of Aeronautics and Astronautics, Fluid and PlasmaDynamics Conference, 16th, Danvers, MA, July 12-14, 1983, AIAA Paper 1983-1738.
[21]Smith, B.L and Glezer, A., "The Formation and Evolution of Synthetic Jets," *Phys. Fluids*, Vol. *10*, 1998, pp. 2281-2297.
[22]R. Wallace, M. Andino, M. Glauser, R. Camphouse, R. Schmit, and J. Myatt, "Flow and Aero-Optics Around a Turret Part II: Surface Pressure Based Proportional Closed Loop Flow Control," 39th Plasmadynamics and Lasers Conference, Seattle, Washington, June 23-26, 2008, AIAA Paper 2008-4217.
[23]R. Wallace, M. Andino, M. Glauser, C. Camphouse, R. Schmit and J. Myatt, "Flow Characteristics of Active Control Around a 3D Turret," 47th AIAA Aerospace Sciences Meeting, Orlando, Florida, Jan. 5-8, 2009, AIAA Paper 2009-573.
[24]Purohit, S. C., Shang, J. S., and Hankey, W. L., Jr., "Numerical simulation of flow around a three-dimensional turret," AIAA and ASME, Joint Thermophysics, Fluids, Plasma and Heat Transfer Conference, 3rd, St. Louis, MO, June 7-11, 1982, AIAA Paper 1982-1020
[25]Jones, M.I. and Bender, E. E.," CFD-based computer simulation of optical turbulence through aircraft flowfields and wakes," AIAA Plasmadynamics and Lasers Conference, 32nd, Anaheim, CA, June 11-14, 2001, AIAA Paper 2001-2798.
[26]P. Morgan and M. Visbal, "Large Eddy Simulation of Flow Around a Turret," 38th Fluid Dynamics Conference and Exhibit, Seattle, Washington, June 23-26, 2008, AIAA Paper 2008-3749.
[27]P. E. Morgan_and M. R. Visbal, "Numerical Simulations Investigating Control of Flow Over a Turret", 47th AIAA Aerospace Sciences Meeting, Orlando, Florida, Jan. 5-8, 2009, AIAA Paper 2009-574.
[28]J. Ladd, M. Mani, and W. Bower, "Validation of Aerodynamic and Optical Computations for the Flow about a Cylindrical/Hemispherical Turret", San-Antonio, 2009, AIAA Paper 2009-4118.
[29]Jurgen Seidel, U.S. Air Force Academy, Colorado Springs, CO, private communication.
[30]K. Wang and M. Wang, "Numerical Simulation of Aero-Optical Distortions by Flow Over a Cylindrical Turret ," 40th AIAA Plasmadynamics and Lasers Conference, San-Antonio, TX, June 22-25, 2009, AIAA Paper 2009-4223.
[31]Philip E. Morgan, Air Force Research Laboratory, Wright-Patterson Air Force Base, OH, private communication.